**51st AIAA Aerospace Sciences Meeting including the New Horizons Forum and Aerospace Exposition**
**07 - 10 January 2013, Grapevine (Dallas/Ft. Worth Region), Texas**

**AIAA 2013-1139**

# LES of a Hydrogen-Enriched
# Lean Turbulent Premixed Flame

Francisco E. Hernández-Pérez [*], Clinton P.T. Groth [†] and Ömer L. Gülder [‡]

*University of Toronto Institute for Aerospace Studies*

*4925 Dufferin Street, Toronto, ON, M3H 5T6, Canada*

   **The application of large-eddy simulation (LES) to the prediction of $H_2$-enriched lean methane-air turbulent premixed combustion is considered. A presumed conditional moment (PCM) subfilter-scale combustion model is coupled with the flame prolongation of intrinsic low-dimensional manifold (FPI) chemistry tabulation technique. The LES and PCM-FPI modelling procedures are then applied to the prediction of laboratory-scale axisymmetric Bunsen-type turbulent premixed flames. Both premixed methane-air and $H_2$-enriched methane-air flames are considered and the predicted solutions are examined and compared to available experimental data. The enriched flame has 20% $H_2$ in terms of mole fraction and lies in the methane-dominated regime. The capability of the LES model to predict the observed behaviour is examined.**

   Hydrogen-hydrocarbon fuel blends appear to be a promising option to synergistically pave the way toward pure hydrogen-based combustion systems while alleviating green-house gas and pollutant emissions related to fossil fuel combustion. The possibility of using hydrogen-enriched hydrocarbon fuels as a means for enabling greater stability of lean premixed flames with significantly reduced emissions of nitrogen oxides is also very appealing.

   While promising, the wide-spread application of hydrogen-enriched hydrocarbon fuels in practical premixed combustion devices has been limited by an incomplete understanding of hydrogen-enriched combustion. In particular, the current understanding, in terms of theoretical and computational models, is unable to fully explain the experimental observations for such flames.

   A number of previous studies have been conducted on the performance and emission characteristics of practical devices using $H_2$-enriched hydrocarbon fuels.[1–4] It has been found that hydrogen enrichment extends the lean stability limit and decreases emissions of carbon monoxide (CO), nitrogen oxides ($NO_x$), and unburned hydrocarbons (UHC) in spark-ignition engines, power-generation gas turbines, and aircraft gas turbines. There have also been several studies focused on fundamental aspects of hydrogen-hydrocarbon flames. It has been reported that $H_2$-enriched flames display higher laminar flame speeds, extended lean flammability limits, and augmented resistance to strain.[5–9] Moreover, experiments in swirl-stabilized burners[10, 11] have been conducted to investigate the stabilization and blowout characteristics of $H_2$-enriched methane-air premixed flames. It has also been shown that the addition of $H_2$ to methane ($CH_4$) extends the flame lean stability limit, allowing stable burner operation at lower flame temperatures and reducing $NO_x$ emissions.

   There have been only a few previous computational studies of multi-dimensional $H_2$-enriched methane-air turbulent premixed flames. Hawkes and Chen[12] performed two-dimensional (2D) direct numerical simulations (DNS) of freely propagating flames in decaying turbulence with complex reduced chemistry (15-step reaction mechanism). Dunstan and Jenkins[13] simulated 2D premixed kernels in decaying turbulence using DNS with detailed chemistry. Day *et al.*[14] performed a 2D study to characterize lean methane-air flames with significant hydrogen addition, including detailed transport and chemical kinetics. Finally, Vreman *et al.*[15] carried out three-dimensional DNS of slot Bunsen flames with tabulated chemistry. In all the DNS simulations cited above, complex chemistry and preferential diffusion were taken into account and their relevance to characterize the flame behaviour were recognized.

---

   [*]Currently at Combustion Technology Research Group, Eindhoven University of Technology, Eindhoven, Netherlands
   [†]Professor, Senior Member AIAA, groth@utias.utoronto.ca
   [‡]Professor, Associate Fellow AIAA, ogulder@utias.utoronto.ca

This study considers the application of large-eddy simulation (LES) and appropriate subfilter-scale (SFS) modelling to the prediction of $H_2$-enriched lean methane-air turbulent premixed combustion. In particular, a presumed conditional moment (PCM) SFS combustion model[16] is coupled with the flame prolongation of intrinsic low-dimensional manifold (FPI) chemistry tabulation technique.[17] The LES and PCM-FPI modelling procedures are then applied to the prediction of laboratory-scale axisymmetric Bunsen-type turbulent premixed flames. Both premixed methane-air and $H_2$-enriched methane-air flames are considered and the predicted solutions are examined and compared to measured data from the experimental study of Halter *et al.*[18] The enriched flame has 20% $H_2$ by volume and lies in the methane-dominated regime. The turbulence intensity for both flames was relatively low and they are expected to correspond to the classical flamelet regime. The capability of the LES model to predict the observed behaviour is examined.

# I.   Large-Eddy Simulation of Turbulent Premixed Flames

The LES framework developed by Hernández-Pérez *et al.*[19, 20] is used for performing this study. The framework is now briefly summarized, along with the PCM-FPI combustion model.

## I.A.   Favre-Filtered Governing Equations

For the LES computations considered here, the Favre-filtered form of the Navier-Stokes equations governing compressible flows of a thermally perfect reactive gaseous mixture, neglecting Dufour, Soret and radiation effects, is used herein to describe the turbulent premixed combustion processes. Relevant flow parameters, $\varphi$, are either filtered using a low-pass spatial filtering procedure or Favre-filtered using a mass-weighted filter to yield $\overline{\varphi}$ or $\widetilde{\varphi}$, respectively. The resulting equations are given by

$$\frac{\partial (\bar{\rho})}{\partial t} + \frac{\partial (\bar{\rho}\tilde{u}_i)}{\partial x_i} = 0 \,, \tag{1}$$

$$\frac{\partial (\bar{\rho}\tilde{u}_i)}{\partial t} + \frac{\partial}{\partial x_j}\left(\bar{\rho}\tilde{u}_i\tilde{u}_j + \delta_{ij}\bar{p} - \check{\tau}_{ij}\right) = \bar{\rho}g_i + A_1 \,, \tag{2}$$

$$\frac{\partial(\bar{\rho}\tilde{E})}{\partial t} + \frac{\partial}{\partial x_i}\left[(\bar{\rho}\tilde{E}+\bar{p})\tilde{u}_i + \check{q}_i\right] - \frac{\partial}{\partial x_j}\left(\check{\tau}_{ij}\tilde{u}_i\right) = \bar{\rho}g_i\tilde{u}_i + B_1 + B_2 + B_3 \,, \tag{3}$$

$$\frac{\partial(\bar{\rho}\tilde{Y}_k)}{\partial t} + \frac{\partial(\bar{\rho}\tilde{Y}_k\tilde{u}_i)}{\partial x_i} + \frac{\partial\check{\mathcal{J}}_{k,i}}{\partial x_i} = \overline{\dot{\omega}}_k + C_1 \,, \tag{4}$$

where $\bar{\rho}$ is the filtered mixture density, $\tilde{u}_i$ is the Favre-filtered mixture velocity, $\bar{p}$ is the filtered mixture pressure, $\tilde{Y}_k$ is the Favre-filtered mass fraction of species $k$, $\tilde{E}$ is the Favre-filtered total mixture energy (including chemical energy) given by $\tilde{E} = \sum_{k=1}^{N}\tilde{Y}_k(\check{h}_k + \Delta h_{f,k}^0) - \bar{p}/\bar{\rho} + \widetilde{u_i u_i}/2$; $\check{h}_k$, $\Delta h_{f,k}^0$ and $\overline{\dot{\omega}}_k$ are the sensible enthalpy, heat of formation and the filtered reaction rate of species $k$, respectively, and $g_i$ is the acceleration due to gravity. The filtered equation of state adopts the form $\bar{p} = \bar{\rho}R\tilde{T}$, assuming that the SFS temperature-species correlation is negligible. Here, $\tilde{T}$ is the Favre-filtered mixture temperature and $R$ is the gas constant. The resolved stress tensor, $\check{\tau}_{ij}$, the resolved total heat flux, $\check{q}_i$, and the resolved species diffusive fluxes, $\check{\mathcal{J}}_{k,i}$, are evaluated in terms of the filtered quantities.

The terms, $A_1$, $B_1$, $B_2$, $B_3$, and $C_1$, arise from the low-pass filtering process and require modelling. These terms are expressed as $A_1 = -\frac{\partial[\bar{\rho}(\widetilde{u_i u_j} - \tilde{u}_i\tilde{u}_j)]}{\partial x_j}$, $B_1 = -\frac{\partial[\bar{\rho}(\widetilde{h u_i} - \check{h}\tilde{u}_i)]}{\partial x_i}$, $B_2 = -\frac{1}{2}\frac{\partial[\bar{\rho}(\widetilde{u_j u_j u_i} - \tilde{u}_j\tilde{u}_j\tilde{u}_i)]}{\partial x_i}$, $C_1 = -\frac{\partial[\bar{\rho}(\widetilde{Y_k u_i} - \tilde{Y}_k\tilde{u}_i)]}{\partial x_i}$, $B_3 = -\frac{\partial\left[\sum_{k=1}^{N}\Delta h_{f,k}^0\bar{\rho}(\widetilde{Y_k u_i} - \tilde{Y}_k\tilde{u}_i)\right]}{\partial x_i}$, and must be modelled for closure of the filtered equation set. The subfilter stresses, $\sigma_{ij} = -\bar{\rho}(\widetilde{u_i u_j} - \tilde{u}_i\tilde{u}_j)$, are modelled using an eddy-viscosity type model with $\sigma_{ij} = 2\bar{\rho}\nu_t(\check{S}_{ij} - \delta_{ij}\check{S}_{ll}/3) + \delta_{ij}\sigma_{ll}/3$. The SFS turbulent viscosity, $\nu_t$, is prescribed herein by using a one-equation model[21] for the SFS turbulent kinetic energy, $k_\Delta$. Standard gradient-based approximations are used in this work for the modelling of the SFS fluxes $B_1$, $B_3$, and $C_1$. The subfilter turbulent diffusion term, $B_2$, is modelled as suggested by Knight *et al.*[22] with $-\bar{\rho}(\widetilde{u_i u_i u_j} - \tilde{u}_i\tilde{u}_i\tilde{u}_j)/2 = \sigma_{ij}\tilde{u}_i$.

## I.B.   PCM-FPI Combustion Model

A primary challenge in the development of LES for turbulent reactive flows is the accurate and reliable modelling of the interaction between turbulence and chemistry and the specification of the filtered reaction

American Institute of Aeronautics and Astronautics

rates, $\overline{\dot{\omega}}_k$. For LES of turbulent premixed combustion, this is further complicated by the large number of species and complexity of the chemical kinetic mechanisms for typical hydrocarbon fuels and the fact that the chemical reactions occur in a thin reacting layer at extremely small scales that are not resolvable on typical LES grids. This places particular importance on the SFS modelling of these terms.

The PCM-FPI[16] is an approach that combines a presumed probability density function (PDF) approach with FPI tabulated chemistry based on prototypical flames with simplified flow geometry.[17] The FPI tabulation technique helps to greatly reduce the costs of performing reactive flow computations involving large chemical kinetic mechanisms and the use of a presumed PDF allows for the economical treatment of the effects of subfilter turbulence on the filtered reaction rates.

For premixed flames of interest here, steady one-dimensional laminar premixed flamelets are used in the construction of the FPI tabulated chemistry. Relevant chemical parameters, $\varphi_j$, such as species mass fractions and/or reaction rates, are related to a single progress of reaction variable, $Y_c$. For a given equivalence ratio, $\phi_0$, the relationship for $\varphi_j = \varphi_j^{\mathrm{FPI}}(\phi_0, Y_c)$ and the progress variable is established by a mapping of computed solutions for steady-state one-dimensional laminar premixed flames expressed as a function of position normal to the flame front on to the $Y_c$-space. For LES of turbulent premixed flames, filtered quantities are then obtained via

$$\tilde{\varphi}_j = \int_0^1 \varphi_j^{\mathrm{FPI}}(c^*)\tilde{P}(c^*)\,\mathrm{d}c^*, \tag{5}$$

where $c$ is the progress variable and $\tilde{P}(c^*)$ is the filtered probability density function of $c$, which needs to be specified. The PDF of $c$ is taken to be a $\beta$-distribution[23, 24] and can be constructed from the resolved or filtered progress variable, $\tilde{c}$, and its SFS variance, $c_{\mathrm{v}} = \widetilde{cc} - \tilde{c}\tilde{c}$. These two variables, $\tilde{c}$ and $c_{\mathrm{v}}$, are directly linked to the progress of reaction $\tilde{Y}_c$ and its SFS variance, $Y_{c_{\mathrm{v}}}$. The filtered progress variable is defined as the filtered progress of reaction normalized by its value at equilibrium: $\tilde{c} = \tilde{Y}_c/Y_c^{\mathrm{Eq}}(\phi_0)$. The variance of $c$ may be obtained from the variance of the progress of reaction, $Y_{c_{\mathrm{v}}} = \widetilde{Y_c Y_c} - \tilde{Y}_c\tilde{Y}_c$ and expressed as $c_{\mathrm{v}} = Y_{c_{\mathrm{v}}}/Y_c^{\mathrm{Eq}^2}(\phi_0)$.

Modelled balance equations are used to determine $Y_c$ and $Y_{c_{\mathrm{v}}}$.[16, 23, 24] The modelled transport equation for $\tilde{Y}_c$ has the form

$$\frac{\partial(\bar{\rho}\tilde{Y}_c)}{\partial t} + \frac{\partial(\bar{\rho}\tilde{u}_i\tilde{Y}_c)}{\partial x_i} = \frac{\partial}{\partial x_i}\left[\bar{\rho}(\check{\mathcal{D}}_{Y_c} + \mathcal{D}_{\mathrm{t}})\frac{\partial\tilde{Y}_c}{\partial x_i}\right] + \overline{\dot{\omega}}_{Y_c}, \tag{6}$$

where $\overline{\dot{\omega}}_{Y_c}$ is a source term due to chemistry, $\check{\mathcal{D}}_{Y_c}$ is the diffusion coefficient associated with $Y_c$, and $\mathcal{D}_{\mathrm{t}}$ is the turbulent diffusion coefficient used to model SFS scalar transport. The transport equation for $Y_{c_{\mathrm{v}}}$ is given by

$$\frac{\partial\left(\bar{\rho}Y_{c_{\mathrm{v}}}\right)}{\partial t} + \frac{\partial\left(\bar{\rho}\tilde{u}_i Y_{c_{\mathrm{v}}}\right)}{\partial x_i} = \frac{\partial}{\partial x_i}\left[\bar{\rho}(\check{\mathcal{D}}_{Y_c} + \mathcal{D}_{\mathrm{t}})\frac{\partial Y_{c_{\mathrm{v}}}}{\partial x_i}\right] + 2\bar{\rho}(\check{\mathcal{D}}_{Y_c} + \mathcal{D}_{\mathrm{t}})\frac{\partial\tilde{Y}_c}{\partial x_i}\frac{\partial\tilde{Y}_c}{\partial x_i}$$
$$-2\overline{\rho\mathcal{D}_{Y_c}\frac{\partial Y_c}{\partial x_i}\frac{\partial Y_c}{\partial x_i}} + 2(\overline{Y_c\dot{\omega}_{Y_c}} - \tilde{Y}_c\overline{\dot{\omega}}_{Y_c}). \tag{7}$$

The scalar dissipation rate of $Y_c$, $\bar{\chi}_{Y_c} = 2\overline{\rho\mathcal{D}_{Y_c}\frac{\partial Y_c}{\partial x_i}\frac{\partial Y_c}{\partial x_i}}$, may be decomposed into resolved and unresolved parts as follows: $\bar{\chi}_{Y_c} = 2\bar{\rho}\check{\mathcal{D}}_{Y_c}\frac{\partial\tilde{Y}_c}{\partial x_i}\frac{\partial\tilde{Y}_c}{\partial x_i} + 2\bar{s}_{\chi_{Y_c}}$. The SFS component is closed with the combined linear relaxation hypothesis and bimodal limit closure proposed by Domingo $et\ al.$,[23] which takes into account that $Y_c$ is a reactive scalar and its gradient is influenced by chemistry.

It is important to remark that a reaction rate can be written as $\dot{\omega} = \rho\dot{\omega}^*$, therefore $\overline{\dot{\omega}} = \bar{\rho}\tilde{\dot{\omega}}^*$ and $\overline{Y_c\dot{\omega}_{Y_c}} = \bar{\rho}\widetilde{Y_c\dot{\omega}_{Y_c}^*}$. The latter is a reaction rate term appearing in the transport equation for $Y_{c_{\mathrm{v}}}$. The terms $\tilde{\dot{\omega}}_{Y_c}^*$ and $\widetilde{Y_c\dot{\omega}_{Y_c}^*}$ are included in the tabulated database. By introducing the segregation factor, $S_c = c_{\mathrm{v}}/(\tilde{c}(1-\tilde{c}))$, a look-up table of filtered quantities $\tilde{\varphi}_j^{\mathrm{PCM}}(\phi_0, \tilde{c}, S_c)$, can be pre-generated for use in subsequent computations.

## I.C.  H$_2$-Enriched Methane-Air Flames

Previous studies by Fiorina $et\ al.$[25] and Galpin $et\ al.$[24] have shown that for FPI tabulated chemistry of methane-air combustion based on steady laminar premixed flamelets, an appropriate choice for the progress of reaction variable is $Y_c = Y_{CO_2} + Y_{CO}$ and it can be sufficient to tabulate data for a rather reduced number of species based on their contributions to mixture mass and energy. In fact, just 10 species:
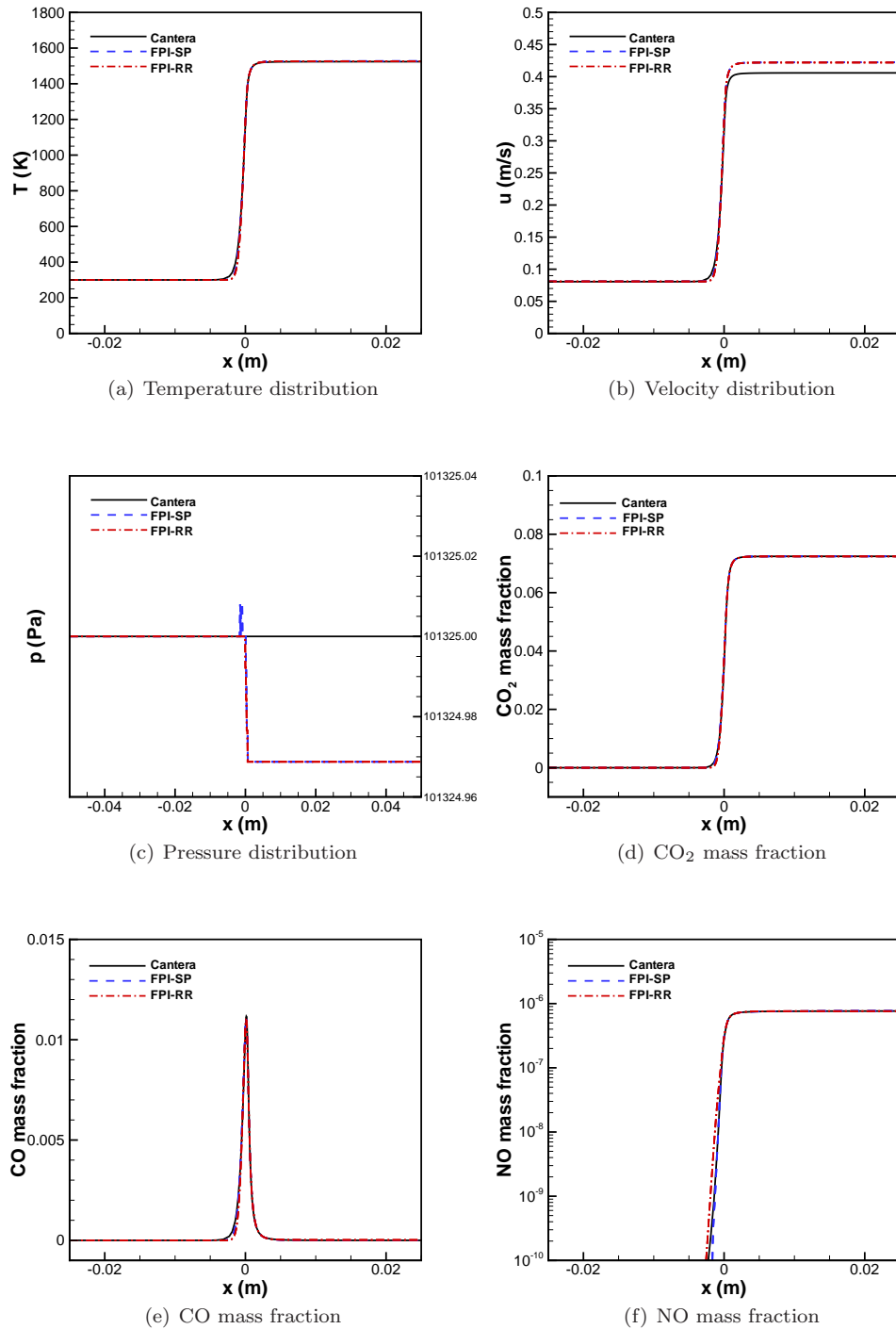
American Institute of Aeronautics and Astronautics

(a) Temperature distribution

(b) Velocity distribution

(c) Pressure distribution

(d) $CO_2$ mass fraction

(e) CO mass fraction

(f) NO mass fraction

**Figure 1. Comparison of predicted temperature, velocity, pressure, and $CO_2$, CO, and NO mass fraction profiles for a one-dimensional premixed laminar $H_2$-$CH_4$-air flame (29% $H_2$ in the fuel) with $\phi = 0.52$ obtained using the proposed PCM-FPI model with $Y_c = Y_{CO_2} + Y_{NO}$ and 14 species to detailed chemical kinetic solutions obtained using Cantera; FPI-SP: reading mass fractions directly; and FPI-RR: transporting the species using reconstructed reaction rates.**

$CH_4, O_2, N_2, H_2O, CO_2, CO, H_2, H, OH$ and $C_2H_2$, are needed to accurately represent the mass and energy of methane-air reactive mixtures.[24] However, in order to improve the prediction of the $H_2$ mass fraction and allow for the prediction of NO in $H_2$-enriched methane-air flames, a revised progress of reaction variable is needed and an enlarged set of species must be tracked. Furthermore, to aid in the treatment of the preferen-

American Institute of Aeronautics and Astronautics

tial diffusion of $H_2$, transport equations for the tracked species are solved directly, along with the equations associated with the progress variable and its variance, using reconstructed filtered reaction rates from the pre-computed FPI look-up tables based on a high Damköler number approximation.[23,24]

In order to assess the FPI tabulation needs for LES of hydrogen enriched methane combustion, steady-state, one-dimensional solutions of $H_2$-enriched methane-air laminar premixed flames were first obtained using the Cantera package[26] with detailed chemistry provided by the GRI-Mech 3.0 chemical kinetics mechanism.[27] GRI-Mech 3.0 has been used previously to obtain good predictions of laminar flame speeds, profiles of major species, $NO_x$ levels, and extinction strain rates in agreement with experimental values.[7,28] The generated solutions were confined to the so-called "methane-dominated regime" and included different levels of enrichment up to a 40% mole fraction of $H_2$ in the blended fuel, with increments of 5%. The equivalence ratio was varied from values near the lean-flammability limit up to two. Note that Di Sarli & Di Benedetto[29] have identified three regimes of laminar burning velocity in terms of the mole fraction of $H_2$ in the fuel, $\varkappa$ ($\varkappa = n_{H_2}/(n_{H_2} + n_{CH_4})$). They are: (i) the methane-dominated combustion ($0 < \varkappa < 0.5$); (ii) the transition regime ($0.5 \leq \varkappa \leq 0.9$); and (iii) the methane-inhibited hydrogen combustion ($0.9 < \varkappa < 1$).

Careful examination and analysis of the laminar premixed flamelet solutions revealed that a suitable single progress of reaction variable for hydrogen-enriched methane combustion, in the methane-dominated regime, is provided by $Y_c = Y_{CO_2} + Y_{NO}$. It was found that this definition of $Y_c$ increases monotonically and can adequately account for the slow chemistry associated with NO for both lean and stoichiometric $H_2$-enriched methane-air premixed flamelets. Note that previous studies have shown that NO must be included in the definition of the progress of reaction variable in order to avoid errors in NO mass fraction that can be introduced when employing a progress variable defined only in terms of major species[30,31] and to properly account for time scales that differ from those of major species.[32,33] Furthermore, based on contributions to mixture mass, energy, and heat release, the species $CH_4$, $CH_3$, $O_2$, O, $N_2$, $H_2O$, $CO_2$, CO, $H_2$, H, and OH were selected, in addition to NO. Two further species, $C_2H_2$ and $NH_3$, were added to allow for elemental mass balance and absorb inconsistencies for C and H. As a result, the number of species included in the FPI look-up tables for the LES of hydrogen-enriched methane-flames considered here was 14 species.

The proposed FPI tabulation method was found to yield accurate solutions for steady, one-dimensional, laminar, premixed $H_2$-$CH_4$-air flames in the methane-dominated regime to within a few percent of the values of the full chemical kinetic solutions, for thermodynamic properties and major and minor species. As an example, consider the comparison of FPI tabulated results obtained using the approach outlined above to detailed chemical kinetic solutions obtained using Cantera given in Figure 1 for a one-dimensional premixed, laminar hydrogen-enriched, methane-air, flame containing 29% $H_2$ (on a molar basis) at atmospheric pressure and having a fresh gas temperature of 300 K. The equivalence ratio for this case is $\phi = 0.52$. The predicted temperature, velocity, pressure, and $CO_2$, CO, and NO mass fraction profiles of the one-dimensional hydrogen-methane-air flame are displayed in the figure. Two sets of results for PCM-FPI approach are given, one based on reading mass fractions directly and the other based on transporting the species with reconstructed reaction rates. The PCM-FPI predictions of the laminar flame speed and burned gas temperature for this enriched flame compare well with those given by Cantera. The predicted profiles of the species $CO_2$, CO, and NO also closely follow the profiles given by the Cantera solutions. In particular, there is a remarkable agreement for the equilibrium NO level, which is less than one part per million (ppm) in this case.

The PCM-FPI look-up tables for hydrogen-enriched methane-air combustion were then generated using pre-computed laminar premixed flamelet solutions obtained using Cantera and GRI-Mech 3.0 convoluted with $\beta$-PDFs for a range of values for the mean and variance of the progress variable. Values for the filtered species mass fractions and filtered quantities $\tilde{\omega}^*_{Y_c}$ and $\widetilde{Y_c \dot{\omega}^*_{Y_c}}$ were stored for retrieval from the look-up tables, which had 138 values of $\tilde{c}$ and 25 values of $S_c$.

## II.    Parallel Finite-Volume Scheme

The Favre-filtered transport equations described above are solved on multi-block hexahedral meshes employing a second-order accurate parallel finite-volume scheme.[19,20,34–37] The inviscid flux at each cell face is evaluated using limited linear reconstruction[38] and Riemann-solver based flux functions,[39,40] while the viscous flux is evaluated utilizing a hybrid average gradient-diamond path method.[41] A standard, explicit, two-stage, second-order-accurate, Runge-Kutta, time-marching scheme is used to integrate forward in time the non-linear, coupled-system, of ordinary differential equations resulting from the finite-volume spatial
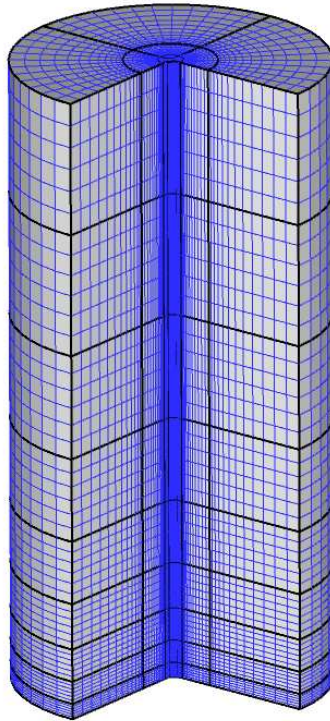
American Institute of Aeronautics and Astronautics

**Figure 2. Cylindrical computational domain and mesh containing 1,638,400 cells used in the LES predictions of the turbulent premixed bunsen flames.**

discretization procedure. Parallel implementation of the solution method has been carried out via domain decomposition using the C++ programming language and the MPI (message passing interface) library.[42, 43]

# III.   LES Results for Bunsen-Type Premixed Flames

LES results for axisymmetric Bunsen-type turbulent premixed methane-air and $H_2$-enriched methane-air flames have been performed. The predicted solutions for both flames are examined and further compared to available data from the experiments of Halter *et al.*[18]

## III.A.   Burner Setup

The Bunsen flames of interest correspond to lean premixed turbulent conditions at an equivalence ratio of $\phi = 0.6$ and atmospheric pressure.[18] For the enriched flame, $H_2$ represents 20% of the blended fuel on a molar basis ($\varkappa = 0.2$). An axisymmetric burner with an inner nozzle diameter of 25 mm was used to generate the premixed turbulent conical flames stabilized by annular pilot flames. The turbulence at the burner exit was characterized by a turbulence intensity $u' = 0.17$ m/s and an integral length scale $L_t = 3$ mm. The mixtures of reactants had a temperature of 300 K and their mean inflow velocity was 2.1 m/s.

In the simulations, a cylindrical domain having a diameter of 0.05 m and a height of 0.1 m was employed and discretized with a grid consisting of 1,638,400 hexahedral cells. The cylindrical computational domain and mesh are show in Figure 2. The pilot flames were approximated by a uniform inflow of hot combustion products at a velocity of 2.73 m/s. For the burner exit, a uniform mean inflow of reactants with superimposed turbulent fluctuations was prescribed. The same turbulence field was used for both the enriched and pure methane flame simulations.

## III.B.   Instantaneous Flame Fronts

Three-dimensional views of the predicted instantaneous flame surfaces for both the pure methane and hydrogen-enriched flames, identified by the isotherm $\tilde{T} = 650$ K, are depicted in Figure 3 corresponding to a physical time $t = 56$ ms, for which a quasi-steady flame structure has been achieved in each case. The
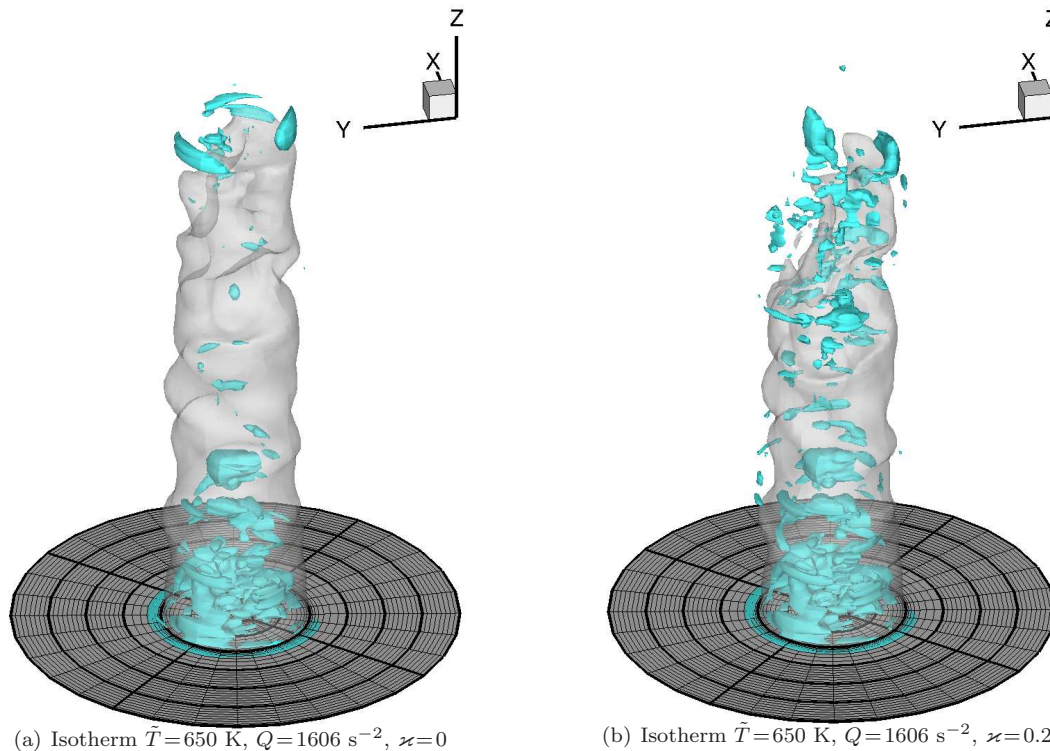
American Institute of Aeronautics and Astronautics

(a) Isotherm $\tilde{T}=650$ K, $Q=1606$ s$^{-2}$, $\varkappa=0$        (b) Isotherm $\tilde{T}=650$ K, $Q=1606$ s$^{-2}$, $\varkappa=0.2$

**Figure 3. Instantaneous iso-surface $\tilde{T}=650$ K of the Bunsen-type flames (light grey) interacting with vortical structures (cyan) identified by $Q=0.5(u'/L_{\mathrm{t}})^2=1606$ s$^{-2}$ at 56 ms. Left: CH$_4$-air flame. Right: H$_2$-CH$_4$-air flame.**

isotherms (light grey) are shown shown interacting with turbulent structures identified by iso-values of the $Q$-criterion, $Q=1606$ s$^{-2}$ (cyan). The $Q$-criterion[44] can be used to visualize the coherent structures of the turbulence. Positive values of $Q$ are associated with regions where vorticity dominates straining.

From Figure 3 it is evident that the simulated flames exhibit a wrinkled surface having a similar structure up to 5 cm above the burner exit. Further downstream, the hydrogen enriched flame displays a higher degree of wrinkling with sharper ridges of negative curvature (curvature is negative in regions that are concave with respect to the unburned gas) and larger pockets of positive curvature, which are more pronounced near the flame tip. The vortical structures identified by the $Q$-criterion are similar in shape and number near the burner exit for both flames. Further downstream, the number of the coherent vortices decreases more rapidly for the pure methane-air flame, whereas a large number of turbulent structures is observed for the H$_2$-enriched flame, particularly in the highly wrinkled region near the flame tip. The addition of H$_2$ would seem to modify the interaction between the flame front and the turbulent field, which can be related to the less diffusive-thermally stable character of the H$_2$-enriched flame. It has been suggested that the diffusive-thermal instability could lead to self-turbulization of flames.[45]

More details of the internal structure of the flames can be seen in Figure 4, where planar cuts of the instantaneous mass fraction distributions of representative species are respectively shown. It is evident that the enriched flame is shorter, which can be ascribed to a faster consumption of the blended fuel. The enriched flame was found to have slightly higher flow temperatures, particularly in regions convex towards the combustible mixture of gases. In addition, more and sharper cusps that protrude the burned gas are observed in the enriched flame. Reduced levels of CO$_2$ (not shown) were also observed in the computed enriched flame. In contrast, the planar cuts of NO mass fractions of Figure 4 display larger amounts of NO in the enriched flame. Areas of larger NO concentrations are localized downstream regions of positive curvature (convex towards the unburned gas) for the enriched case. These regions also coincide with areas of high temperature. The planar cuts of CO mass fractions show an intensified production of CO for the enriched flame in the highly wrinkled region near the flame tip, around the centerline. However, no significant difference of CO levels is noticeable in the fully burned gas zones of the two flames from these contours.
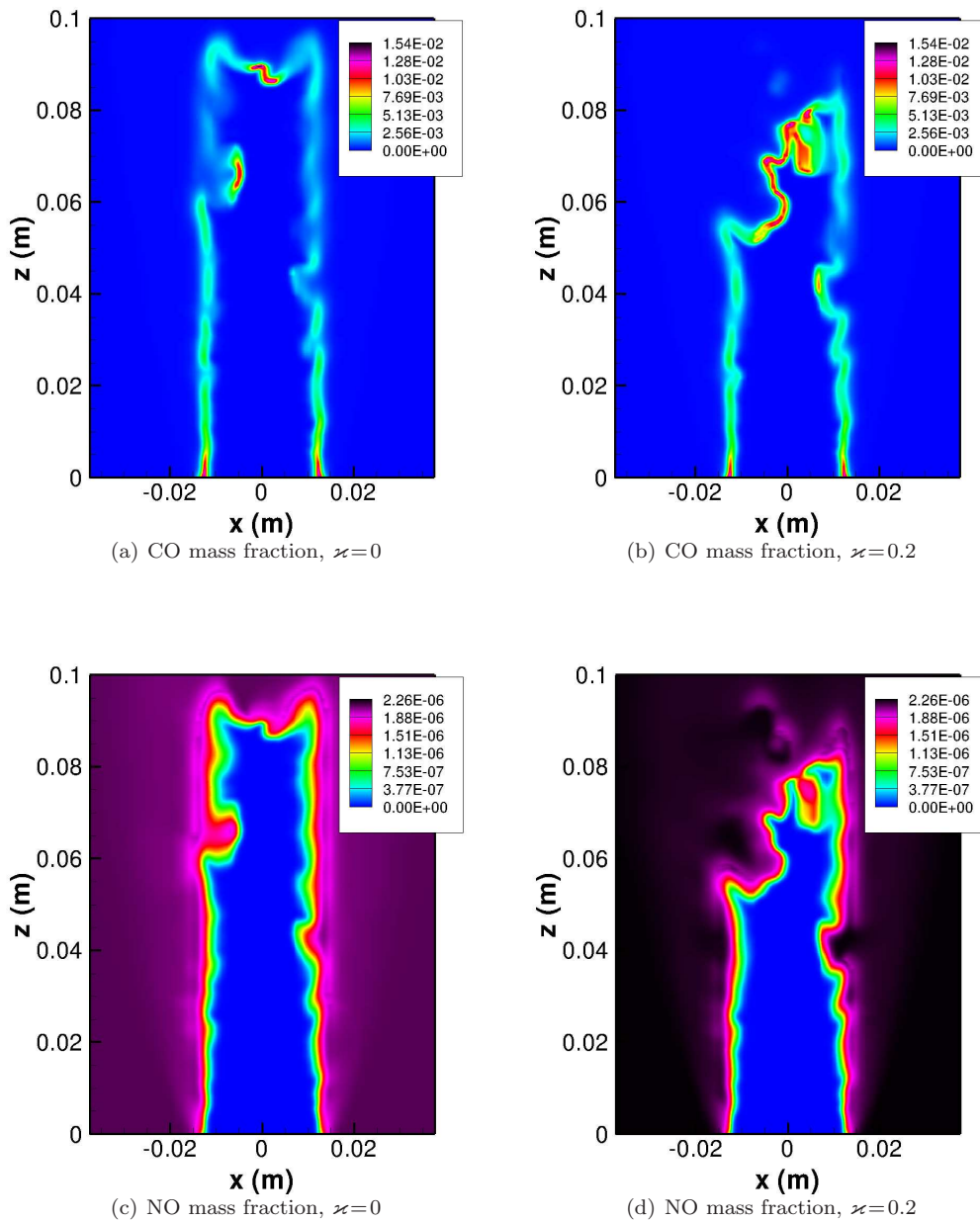
American Institute of Aeronautics and Astronautics

(a) CO mass fraction, $\varkappa=0$      (b) CO mass fraction, $\varkappa=0.2$

(c) NO mass fraction, $\varkappa=0$      (d) NO mass fraction, $\varkappa=0.2$

**Figure 4. Planar cuts of the instantaneous CO and NO mass fraction distributions of the Bunsen-type flames at 56 ms. Plane $y=0$. Left: CH$_4$-air flame. Right: H$_2$-CH$_4$-air flame.**

## III.C. Average Flame Structure

To compare the numerical results with the experimental data of Halter *et al.*,[18] a time-average of the LES solutions was performed over 70 ms (from 30 ms to 100 ms) using 71 instantaneous snapshots of each solution. Moreover, 2D slices of the resolved LES temperature field were extracted and processed to calculate progress variable fields based on temperature. The experimental flame brush was calculated using 500 Mie scattering images of oil droplets seeded in the fresh mixture of reactants.[18] The images were binarised and an edge-finding algorithm was applied to each instantaneous image to determine the progress variable maps. The resolution of the Mie scattering imaging procedure was 110 $\mu$m/pixel.

The experimental and numerical flame brushes are given in Figure 5. Although clear differences between the experimental and numerical results can be seen, both the experiments and the simulations show a
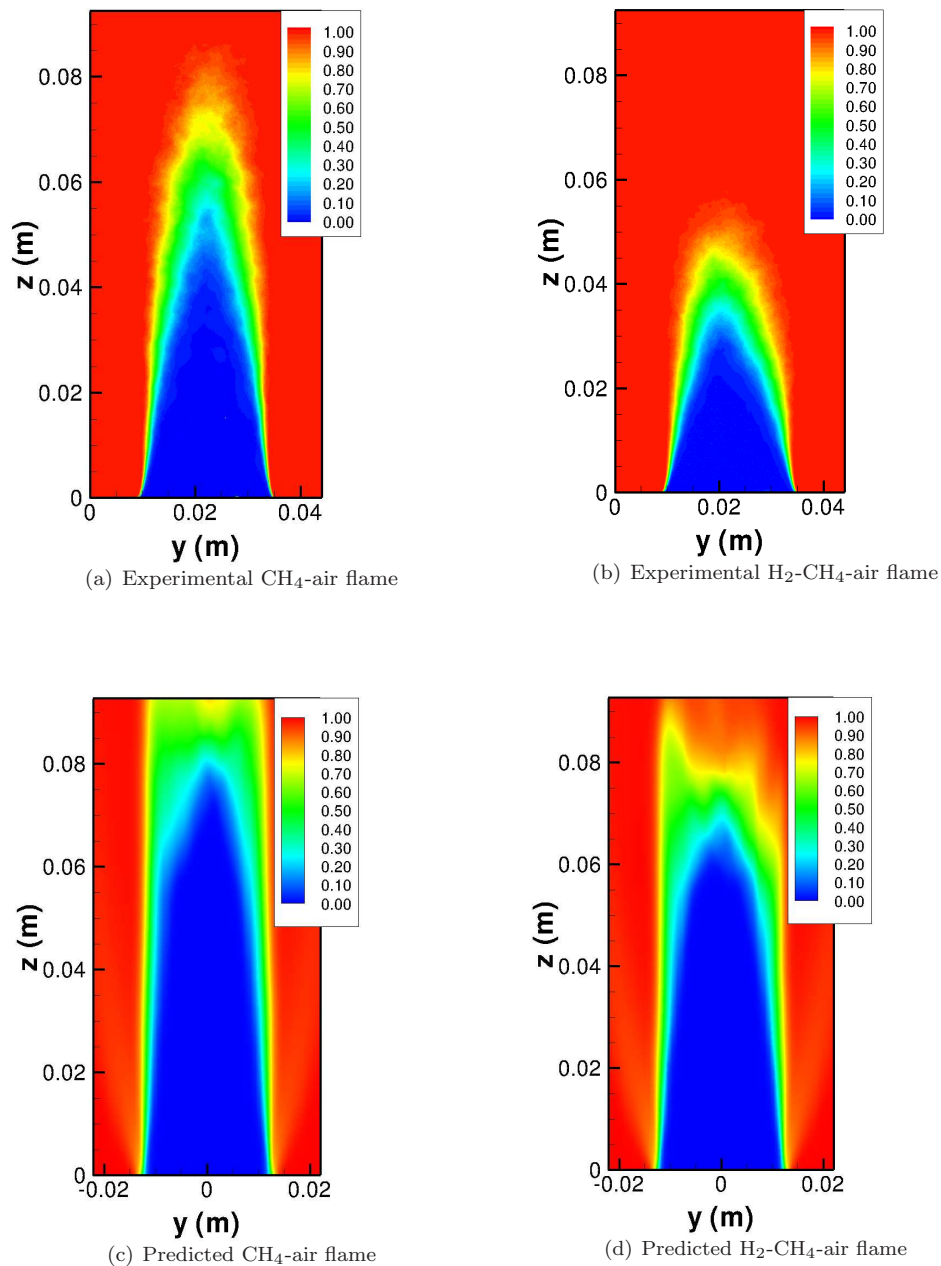
American Institute of Aeronautics and Astronautics

(a) Experimental $CH_4$-air flame

(b) Experimental $H_2$-$CH_4$-air flame

(c) Predicted $CH_4$-air flame

(d) Predicted $H_2$-$CH_4$-air flame

**Figure 5. Comparison of experimental and predicted temperature-based flame brushes for the Bunsen-type $CH_4$-air and $H_2$-$CH_4$-air flames.**

decrease in the flame height (36% and 18%, respectively, computed from the temperature-based progress variable $c_T = 0.1$ contour and evaluated at the centerline[18]) when hydrogen is added to methane, indicating a higher global burning rate for the enriched flame. It can also be observed that the predicted flames are taller that their experimental counterparts. It is worth noting that pockets of unburned gas were neglected (i.e., they were treated as burned gas) in the image analysis of Halter.[18] The presence of pockets of unburned gas near and above the flame tip in the instantaneous images would increase the height of the ensemble-averaged flame front. Therefore, the actual flame brushes are expected to be somewhat taller than those shown in Figure 5.
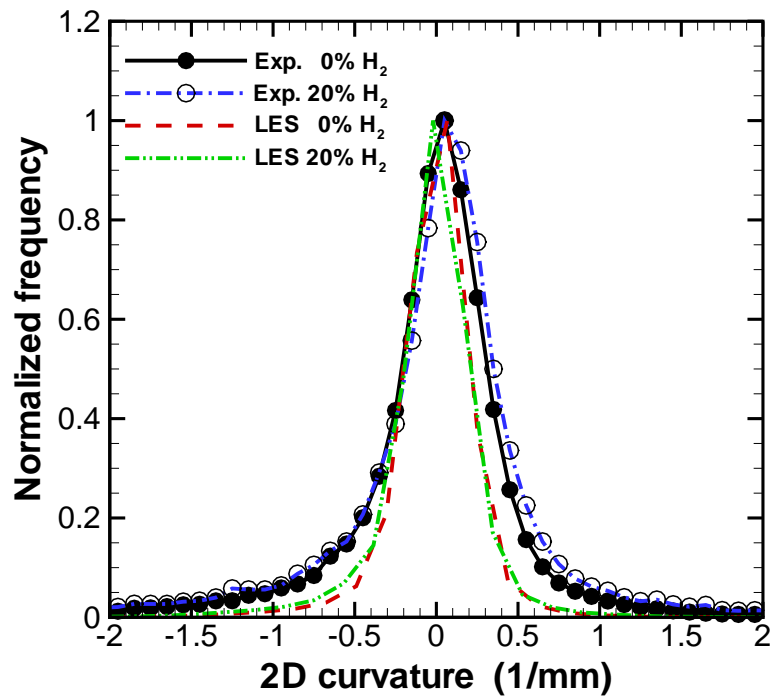
American Institute of Aeronautics and Astronautics

**Figure 6. PDF of 2D curvature corresponding to a progress variable $c_T = 0.5$ for the Bunsen-type CH$_4$-air and H$_2$-CH$_4$-air flames.**

Two-dimensional curvature was also extracted from instantaneous unfiltered experimental images and slices of the numerical solutions. The curvature PDFs from the experimental data and the LES solutions associated to the $c_T = 0.5$ contour are shown in Figure 6. The PDFs display a Gaussian-type shape centred around zero, with the PDF corresponding to the predicted enriched flame being slightly skewed towards negative values of curvature. The PDFs corresponding to the LES simulations are narrower, owing to a smaller resolution of the flame front as compared to the experimental flame front images. It is apparent that the addition of hydrogen leads to slightly broader PDFs, in both the experiments and the simulations, with higher probabilities of finding larger curvatures for the enriched flame. This indicates that more small-scale wrinkling is present in the enriched flame.

## IV.  Conclusions

In summary, the LES simulations of axisymmetric Bunsen-type turbulent premixed methane-air and H$_2$-enriched methane-air flames predicted similar qualitative trends to those found in the experiments of Halter *et al.*[18] for flame height and curvature. The enriched flame was shorter, which is attributed to a faster consumption of the blended fuel. The curvature PDFs displayed a Gaussian-type shape centred around zero. In both the experiments and the simulations, the addition of hydrogen lead to slightly broader PDFs. Furthermore, the hydrogen enriched flame displayed a higher degree of wrinkling with sharper ridges of negative curvature and larger pockets of positive curvature, which were more pronounced near the flame tip. This behaviour has been associated with preferential diffusion effects and the less diffusive-thermally stable character of the H$_2$-enriched flame. In addition, reduced levels of CO$_2$ and increased levels of NO emissions were predicted for the enriched flame, and a slight increase in the CO levels in areas of fully burned gas was exhibited in the predicted enriched flame. Overall, the proposed treatment for the PCM-FPI combustion model, in terms of progress variable and tabulated data, appears to perform well for enriched methane flames in the methane-dominated regime. Further study is warranted for a wider class of flames.

American Institute of Aeronautics and Astronautics

# Acknowledgments

# References

[1] Nagalingam, B., Duebel, F., and Schmillen, K., "Performance study using natural gas, hydrogen-supplemented natural gas and hydrogen in AVL research engine," *Int. J. Hydrogen Energy*, Vol. 8, 1983, pp. 715–720.

[2] Bell, S. R. and Gupta, M., "Extension of the lean operating limit for natural gas fueling of spark ignited engine using hydrogen blending," *Combustion Science and Technology*, Vol. 123, 1997, pp. 23–48.

[3] Bauer, C. G. and Forest, T., "Efect of hydrogen addition on the performance of methane-fueled vehicles. Part I: efect on S.I. engine performance," *Int. J. Hydrogen Energy*, Vol. 26, 2001, pp. 71–77.

[4] Kumar, M. S., Ramesh, A., and Nagalingam, B., "Use of hydrogen to enhance the performance of a vegetable oil fuelled compression ignition engine," *Int. J. Hydrogen Energy*, Vol. 28, 2003, pp. 1143–1154.

[5] Yu, G., Law, C. K., and Wu, C. K., "Laminar flame speeds of hydrocarbon + air mixtures with hydrogen addition," *Combust. Flame*, Vol. 63, 1986, pp. 339–347.

[6] Gauducheau, J. L., Denet, B., and Searby, G., "A Numerical Study of Lean $CH_4/H_2$/Air Premixed Flames at High Pressure," *Combust. Sci. Tech.*, Vol. 137, 1998, pp. 81–99.

[7] Ren, J.-Y., Qin, W., Egolfopoulos, F. N., and Tsotsis, T. T., "Strain-Rate Effects on Hydrogen-Enhanced Lean Premixed Combustion," *Combust. Flame*, Vol. 124, 2001, pp. 717–720.

[8] Jackson, G. S., Sai, R., Plaia, J. M., Boggs, C. M., and Kiger, K. T., "Influence of $H_2$ on the response of lean premixed $CH_4$ flames to high strained flows," *Combust. Flame*, Vol. 132, 2003, pp. 503–511.

[9] Guo, H., Smallwood, G. J., Liu, F., Ju, Y., and Gülder, O. L., "The effect of hydrogen addition on flammability limit and $NO_x$ emission in ultra-lean counterflow $CH_4$/Air premixed flames," *Proc. Combust. Inst.*, Vol. 30, The Combustion Institute, 2005, pp. 303–311.

[10] Schefer, R. W., "Hydrogen Enrichment for Improved Lean Flame Stability," *Int. J. Hydrogen Energy*, Vol. 28, 2003, pp. 1131–1141.

[11] Kim, H. S., Arghode, V. K., and Gupta, A. K., "Flame characteristics of hydrogen-enriched methane-air premixed swirling flames," *Int. J. Hydrogen Energy*, Vol. 34, 2009, pp. 1063–1073.

[12] Hawkes, E. R. and Chen, J. H., "Direct numerical simulation of hydrogen-enriched lean premixed methane-air flames," *Combust. Flame*, Vol. 138, 2004, pp. 405–436.

[13] Dunstan, T. D. and Jenkins, K. W., "The efects of hydrogen substitution on turbulent premixed methane-air kernels using direct numerical simulation," *Int. J. Hydrogen Energy*, Vol. 34, 2009, pp. 8389–8404.

[14] Day, M. S., Gao, X., and Bell, J. B., "Properties of lean turbulent methane-air flames with significant hydrogen addition," *Proc. Combust. Inst.*, Vol. 33, The Combustion Institute, 2011, pp. 1601–1608.

[15] Vreman, A. W., van Oijen, J. A., de Goey, L. P. H., and Bastiaans, R. J. M., "Direct numerical simulation of hydrogen addition in turbulent premixed Bunsen flames using flamelet-generated manifold reduction," *Int. J. Hydrogen Energy*, Vol. 34, 2009, pp. 2778–2788.

[16] Domingo, P., Vervisch, L., Payet, S., and Hauguel, R., "DNS of a premixed turbulent V flame and LES of a ducted flame using a FSD-PDF subgrid scale closure with FPI-tabulated chemistry," *Combust. Flame*, Vol. 143, 2005, pp. 566–586.

[17] Gicquel, O., Darabiha, N., and Thévenin, D., "Laminar premixed hydrogen/air counterflow flame simulations using Flame Prolongation of ILDM with differential diffusion," *Proc. Combust. Inst.*, Vol. 28, The Combustion Institute, 2000, pp. 1901–1908.

[18] Halter, F., Chauveau, C., and Gökalp, I., "Characterization of the effects of hydrogen addition in premixed methane/air flames," *Int. J. Hydrogen Energy*, Vol. 32, 2007, pp. 2585–2592.

[19] Hernández-Pérez, F. E., *Subfilter Scale Modelling for Large Eddy Simulation of Lean Hydrogen-Enriched Turbulent Premixed Combustion*, Ph.D. thesis, University of Toronto, April 2011.

[20] Hernández-Pérez, F. E., Yuen, F. T. C., Groth, C. P. T., and Gülder, O. L., "LES of a Laboratory-Scale Turbulent Premixed Bunsen Flame Using FSD, PCM-FPI and Thickened Flame Models," *Proc. Combust. Inst.*, Vol. 33, 2011, pp. 1365–1371.

[21] Yoshizawa, A., "Statistical theory for compressible turbulent shear flows, with the application to subgrid modeling," *Phys. Fluids A*, Vol. 29, 1986, pp. 2152–2164.

[22] Knight, D., Zhou, G., Okong'o, N., and Shukla, V., "Compressible Large Eddy Simulation Using Unstructured Grids," Paper 98-0535, AIAA, January 1998.

[23] Domingo, P., Vervisch, L., and Veynante, D., "Large-eddy simulation of a lifted methane jet flame in a vitiated coflow," *Combust. Flame*, Vol. 152, 2008, pp. 415–432.

[24] Galpin, J., Naudin, A., Vervisch, L., Angelberger, C., Colin, O., and Domingo, P., "Large-eddy simulation of a fuel-lean premixed turbulent swirl-burner," *Combust. Flame*, Vol. 155, 2008, pp. 247–266.

[25] Fiorina, B., Gicquel, O., Vervisch, L., Carpentier, S., and Darabiha, N., "Premixed turbulent combustion modeling using tabulated detailed chemistry and PDF," *Proc. Combust. Inst.*, Vol. 30, The Combustion Institute, 2005, pp. 867–874.

[26] Goodwin, D. and Moffat, H. K., "Cantera," Available at http://code.google.com/p/cantera/.

[27] Smith, G. P., Golden, D. M., Frenklach, M., Moriarty, N. W., Eiteneer, B., Goldenberg, M., Bowman,

C. T., Hanson, R. K., Song, S., Gardiner, W. C., Lissianski, V. V., and Qin, Z., "GRI-Mech 3.0," Available at http://www.me.berkeley.edu/gri_mech/.

[28]Ren, J.-Y., Qin, W., Egolfopoulos, F. N., Mak, H., and Tsotsis, T. T., "Methane reforming and its potential effect on the efficiency and pollutant emissions of lean methane–air combustion," *Chem. Eng. Sci.*, Vol. 56, 2001, pp. 1541–1549.

[29]di Sarli, V. and di Benedetto, A., "Laminar burning velocity of hydrogen–methane/air premixed flames," *Int. J. Hydrogen Energy*, Vol. 32, 2007, pp. 637–646.

[30]Bradley, D., Gaskell, P. H., Gu, X. J., Lawes, M., and Scott, M. J., "Premixed turbulent flame instability and NO formation in a lean-burn swirl burner," *Combust. Flame*, Vol. 115, 1998, pp. 515–538.

[31]Godel, G., Domingo, P., and Vervisch, L., "Tabulation of $NO_x$ chemistry for large-eddy simulation of non-premixed turbulent flames," *Proc. Combust. Inst.*, Vol. 32, The Combustion Institute, 2009, pp. 1555–1561.

[32]Hill, S. C. and Smoot, L. D., "Modeling of nitrogen oxides formation and destruction in combustion systems," *Prog. Energy Combust. Sci.*, Vol. 26, 2000, pp. 417–458.

[33]Frassoldati, A., Frigerio, S., Colombo, E., Inzoli, F., and Faravelli, T., "Determination of $NO_x$ emissions from strong swirling confined flames with an integrated CFD-based procedure," *Chem. Eng. Sci.*, Vol. 60, 2005, pp. 2851–2869.

[34]Gao, X. and Groth, C. P. T., "Parallel Adaptive Mesh Refinement Scheme for Three-Dimensional Turbulent Non-Premixed Combustion," Paper 2008-1017, AIAA, January 2008.

[35]Gao, X. and Groth, C. P. T., "A Parallel Solution Adaptive Method for Three-Dimensional Turbulent Non-Premixed Combusting Flows," *J. Comput. Phys.*, Vol. 229, 2010, pp. 3250–3275.

[36]Lin, W., Hernández-Pérez, F. E., Groth, C. P. T., and Gülder, O. L., "Comparison of Subfilter Scale Models for LES of Turbulent Premixed Flames," Paper 2008-1048, AIAA, January 2008.

[37]Lin, W., *Large-Eddy Simulation of Premixed Turbulent Combustion Using Flame Surface Density Approach*, Ph.D. thesis, University of Toronto, 2010.

[38]Barth, T. J., "Recent Developments in High Order K-Exact Reconstruction on Unstructured Meshes," Paper 93-0668, AIAA, January 1993.

[39]Roe, P. L., "Approximate Riemann Solvers, Parameter Vectors, and Difference Schemes," *J. Comput. Phys.*, Vol. 43, 1981, pp. 357–372.

[40]Liou, M.-S., "A Sequel to AUSM, Part II: AUSM$^{+}$-up for all Apeeds," *J. Comput. Phys.*, Vol. 214, 2006, pp. 137–170.

[41]Mathur, S. R. and Murthy, J. Y., "A Pressure-Based Method for Unstructured Meshes," *Numerical Heat Transfer*, Vol. 31, 1997, pp. 191–215.

[42]Gropp, W., Lusk, E., and Skjellum, A., *Using MPI*, MIT Press, Cambridge, Massachussets, 1999.

[43]Gropp, W., Lusk, E., and Thakur, R., *Using MPI-2*, MIT Press, Cambridge, Massachussets, 1999.

[44]Hunt, J. C. R., Wray, A. A., and Moin, P., "Eddies, stream, and convergence zones in turbulent flows," *Annual Research Briefs*, Center for Turbulence Research, 1988.

[45]Sivashinsky, G. I., "Instabilities, pattern formation, and turbulence in flames," *Ann. Rev. Fluid Mech.*, Vol. 15, 1983, pp. 179–199.

American Institute of Aeronautics and Astronautics